 doi:10.20944/preprints202105.0483.v1

Calculation of the flux density function for protein crystals from small scale settling and filtration experiments

Benjamin Radel[a,*], Tu Hoang Nguyen[a], Hermann Nirschl[a]

[a]*Karlsruhe Institute of Technology (KIT), Institute of Mechanical Process Engineering and Mechanics, 8 Strasse am Forum, Karlsruhe 76131, Germany*

Abstract

Development and engineering of protein crystals regarding mechanical stability and crystallizability occurs on a small scale. Later in the process chain of industrial production however, filtration properties are important to separate the crystals from mother liquor. Many protein crystals are sensitive to mechanical stress which is why it is important to know the filtration behavior early on. In this study we analyze settling and filtration behavior of isometric, rod-like and needle shaped lysozyme and rod-like alcohol dehydrogenase (ADH) crystals on a small scale using an optical analytical centrifuge. Needle shaped lysozyme and rod-like ADH crystals show compressible material behavior. With the results from settling and filtration experiments the flux density function is calculated and modeled which can be used to describe the whole settling and permeation process in dependency of the solids volume fraction. This is also an issue for simulations of industrial processes.

Keywords: Filtration, Flux density function, Protein crystals

1. Introduction

The improvement of bulk protein crystallization for purification or formulation is subject of current research. Crystalline proteins are advantageous compared to dissolved or amorph solids because of their extended shelf life or modified drug release properties [1, 2]. The implementation of a crystallization step in the downstream process chain for protein purification and formulation is discussed in literature by Hubbuch et al. [3] and Hekmat [4]. In recent research either the proteins were modified to improve or enable crystallization, or the crystals itself were altered to enhance mechanical stability [5–7]. Nowotny et al. [5] and Hermann et al. [6] identified crucial amino acids for crystallization in the sequence of the protein alcohol dehydrogenase from *Lactobacillus brevis* in a rational crystal engineering approach using a molecular dynamics model. They confirmed their findings with experimental results for three different mutants with improved crystallizability. Grob et al. [8] demonstrated the applicability of technical crystallization in downstream processing with the protein alcohol dehydrogenase. Kubiak et al. [7] used cross-linking of crystals, which drastically enhanced the crystal's ability to withstand mechanical stress. Kubiak et al. [9] reported anisotropic mechanical properties for cross-linked halohydrin dehalogenase crystals and investigated the effect of cross-linking time on crystals hardness and Young's modulus. Crystal breakage at pressures below 1×10^5 Pa for native crystals has been previously reported by Cornehl et al. [10] which negatively affects the filtration behavior of such particle systems [11].

Filtration is a common procedure to separate solids from a liquid for further processing [12]. Hence, filtration is also suitable to separate protein crystals from saturated mother liquor. Cake forming filtration processes are well characterized and several models describing filtration parameters and cake properties may be found in literature [13–16]. Existing traditional filtration setups are changing to account for challenges in pharmaceutical applications (integrated compact filtration devices [17]) or to reduce the required amount of sample in early product development. Performing standard laboratory experiments to characterize filtration properties, e. g. according to VDI 2762 [18], usually require liters of suspension or fluid. Those amounts are not available in early product development like protein or crystal modification. This research is conducted on a much smaller scale ranging from micro- to milliliters. Investigating filtration properties of protein crystals on an early stage of process development therefore requires a much smaller laboratory setup. Radel et al. [19] introduced a downscaled filtration setup for an optical laboratory centrifuge which is based on the setup published by Loginov et al. [20] for investigating filtration properties at a small scale.

To model the settling and filtration process, the flux density function –originally introduced for flocculated suspensions– can be used. The flux density function for settling processes was introduced by Kynch [21]. Calculating values for the flux density function for solids volume fractions above the gel point from permeability data of filter cakes or sediments was added by Bürger et al. [22]. The gel point describes the transition from a suspension to a particulate network. The flux density function is only dependent on the solids volume fraction and describes the settling and permeation properties

*Corresponding author
Email address: benjamin.radel@kit.edu (Benjamin Radel)

Preprints (www.preprints.org) | NOT PEER-REVIEWED | Posted: 20 May 2021 doi:10.20944/preprints202105.0483.v1

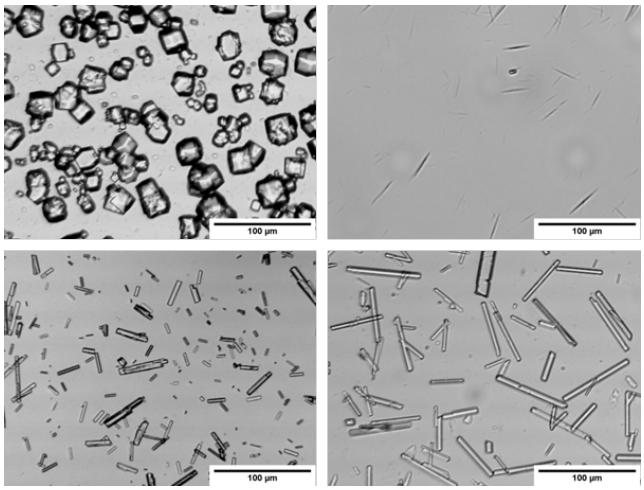

Figure 1: Microscopy images of the used protein crystals; Top left: isometric lysozyme, top right: needle shaped lysozyme, bottom left: rod-like lysozyme, bottom right: ADH crystals

of a particle system. In numerical simulations of settling or filtration processes, the flux density function combined with the compressible yield stress are useful input parameters to model the whole separation process.

2. Methods

2.1. Particle System

This study considers three different lysozyme crystal systems (isometric, rod-like and needle shaped) and the commercially not available crystal system alcohol dehydrogenase (ADH) from *Lactobacillus brevis*. Precipitated hen egg-white lysozyme is obtained from Ovobest (Germany), the ADH enzyme is kindly provided by Prof. Weuster-Botz from the institute of biochemical engineering at the Technical University of Munich. Exemplary microscopy images of the crystal systems can be seen in Fig. 1.

The crystallized proteins for needle shaped lysozyme, rod-like lysozyme and ADH are kindly provided by Prof. Kind from the institute of thermal process engineering at Karlsruhe Institute of Technology. Those crystals are produced using a low temperature vacuum evaporation process described in detail by Barros Groß, Kind [23, 24]. Whereas isometric and ADH crystals grow at 24 °C, the rod-like lysozyme crystals are produced at 35 °C.

The production of isometric lysozyme crystals is achieved with displacement crystallization and hence requires two stock solutions. Stock solution A is a 25 mmol acidic acid buffer at pH 4.0. Stock solution B contains 80 g L^{-1} NaCl additionally. 100 g L^{-1} lysozyme are dissolved in 125 mL stock solution A and gently stirred with a blade stirrer at 350 rpm. A membrane pump adds 125 mL stock solution B to the mixture at a rate of 1 mL min^{-1}. The whole crystallization process takes about 16 h to reduce the supersaturation and to reach equilibrium.

Additionally, for the analysis of filtration behavior, the particle and supernatant properties density and viscosity must be known. Those parameters are shown in Table 1. The density of crystalline lysozyme is obtained from Kundrot, Richards [25]. In house measurements with Mettler Toledo (USA) Densito 30PX yield the liquid densities using the oscillating tube method according to EN ISO 15212-1 [26]. The solid density of ADH is measured with gas pycnometer MP 1305 (Micromeritics GmbH, Germany) [27]. Liquid viscosity is obtained with falling sphere viscometry.

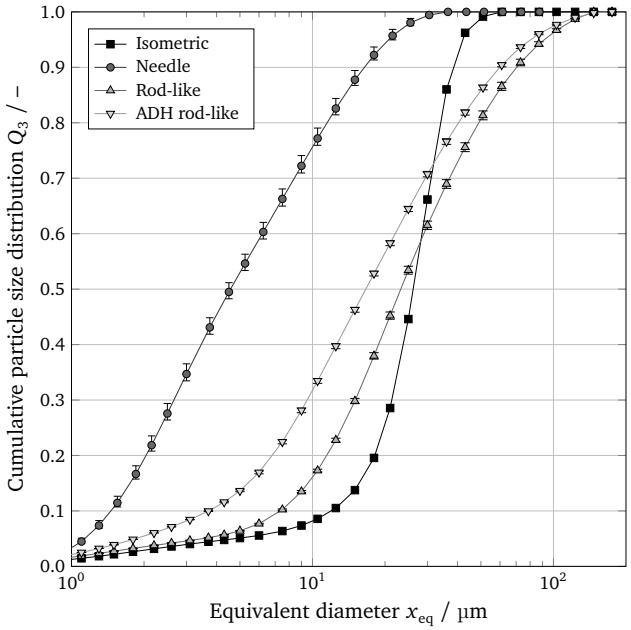

Figure 2: Cumulative particle size distributions of the crystalline particles obtained with laser diffraction

Figure 2 shows the cumulative particle size distributions Q_3 of each crystalline system measured in suspension with Sympatec (Germany) Helos laser diffractometer H0309 using the laser diffraction method. Due to its measurement principle, laser diffraction gives the equivalent diameter of a sphere, which obviously is only a rough characterization for elongated particles like needles or rods. However, it is still possible to compare the different particle systems relative to each other. Error bars in Fig. 2 indicate the minimum and maximum value of repeated measurements.

2.2. Settling experiments

The settling velocity of particle collectives depends on the solids volume fraction ϕ, which is defined as

$$\phi = \frac{V_s}{V_T} = \frac{V_s}{V_s + V_p} = 1 - \epsilon, \tag{1}$$

Table 1: Material properties of the crystalline systems

Particle system	Density solid ρ_s kg m^{-3}	Density liquid ρ_l kg m^{-3}	Dyn. Viscosity η mPa s
Lysozyme isometric	1236	1023	1.19
Lysozyme rod-like	1236	1023	1.19
Lysozyme needle	1236	1029	1.19
ADH	1250	1026	1.92

Preprints (www.preprints.org) | NOT PEER-REVIEWED | Posted: 20 May 2021 doi:10.20944/preprints202105.0483.v1

with V_s, V_T, V_p as the solids volume, total volume and volume of the void. ϵ is the porosity which is commonly used in the characterization of particulate networks. For low solids volume fractions the particles settle individually depending on density (ρ) and diameter (x). In the case of spherical particles, Reynolds numbers below 0.25 and Newtonian fluids the velocity equals

$$v_s = \frac{(\rho_s - \rho_l) g x^2}{18\eta} \tag{2}$$

which is the Stokes law. [12] With increasing solids volume fraction, the settling regime changes from single particle over swarm to zone settling. In the last regime, all particles have the same settling velocity independent of their diameter. Typically, a sharp transition of clear liquid to suspension, the settling front, develops. [12, 28] To account for the influence of solids volume fraction on the settling velocity several enhancements to Stokes law in Eq. 2 have been introduced in the literature. One common amendment was by Richardson, Zaki [28]

$$v_{rz} = v_s (1-\phi)^m \tag{3}$$

with the parameter m being a function of the Reynolds number. For laminar conditions m equals 4.65.

By tracking the settling front over time, settling velocity of the particle system is easily characterized. A typical experiment uses settling columns with different initial solids volume fractions as depicted in Fig. 3. It is crucial to measure the settling velocity at the beginning of the settling process, because during settling the solids volume fraction in the suspension increases and becomes inhomogeneous. Hence, the solids volume fraction is only known at the very beginning of the experiment. The position of the settling front is tracked over time. For particle systems settling quickly, the device LUMiReader® (LUM GmbH, Germany) is used. The sample is filled into a cuvette and placed in the sample holder. Light transmission over the cuvette height is measured to track the settling front. Particle systems settling slowly however, are

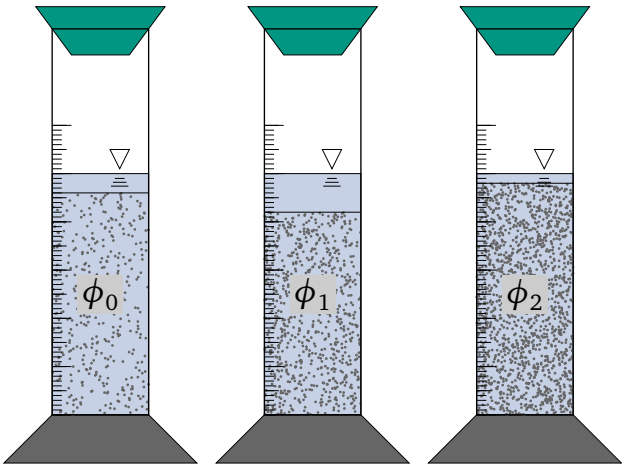

Figure 3: Settling columns with different initial solid volume fractions after the same settling time

measured using the analytical optical centrifuge LUMiSizer® (LUM GmbH, Germany) at 500 rpm. The working principal is basically the same but due to higher centrifugal forces, the process is much quicker. For the detailed measurement principle please refer to Lerche, Sobisch [29]. Because the settling velocity in the centrifugal field is higher than in earth gravity, we have to divide the obtained settling velocity from the centrifuge by the relative centrifugal acceleration

$$Z = \frac{r_1 + r_0}{2} \frac{\omega^2}{g}. \tag{4}$$

To create solutions with different solids volume fractions, addition or removal of supernatant from the initial stock solution is necessary. Adding supernatant to the crystal stock solution creates crystal suspensions with lower solids volume fractions. To increase solids volume fraction, a defined volume of supernatant was removed from samples centrifugated at low speeds. Thus, no crystal breakage occurs and redispersing the sediment in remaining supernatant is easy. The optical centrifuge holds up to twelve cuvettes enabling the parallel measurement of the settling front for different solids volume fractions. One important requirement is a clear detectable settling front. Otherwise, it is not possible to determine a single settling velocity. Per measurement approximately 1.0 mL of sample is required.

2.3. Filtration experiments

Filtration is a common technique to separate solids from liquids. In dead end cake filtration the particles are hold back by a porous filter medium, like a porous membrane or a filter cloth while the filtrate passes through the filter medium. The retained particles on the filter medium first form a thin layer and build particle bridges, then a filter cake. This filter cake may retain particles even smaller than the pores of the filter medium. Often, the chosen pore size of the filter medium is larger than the particles to avoid clogging and to keep the filter medium resistance (R_m) low. The danger of clogging becomes maximal if the pore size is in the same range as the particle sizes. [12] In this study, however, the chosen pore size is much smaller than the particles to avoid filtrate pollution and clogging.

Darcy's law connects the pressure drop Δp, filter area (A_m), volume flow rate ($\dot{V}$) and the resistance against permeation (R) with each other. For constant pressure filtration Darcy's law follows

$$\frac{\mathrm{d}V}{\mathrm{d}t} = \frac{\Delta p A_m}{\eta R}. \tag{5}$$

The resistance is typically split into the resistance of the filter medium (R_m) and resistance of the filter cake (R_c). The resistance of the filter cake changes with its height (h). Thus, for better comparability, the resistance is normalized with either its height or its mass

$$\alpha_h = \frac{R_c}{h_c} = K^{-1}, \tag{6}$$

$$\alpha_m = \frac{\alpha_h}{\phi_c \rho_s}. \tag{7}$$

Preprints (www.preprints.org) | NOT PEER-REVIEWED | Posted: 20 May 2021 doi:10.20944/preprints202105.0483.v1

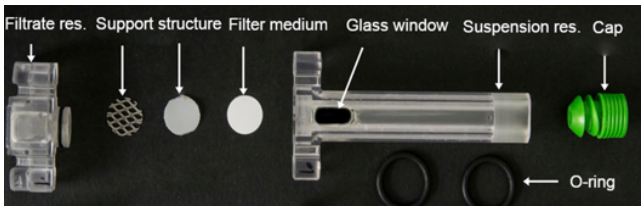

Figure 4: 3D printed filtration cell

The reciprocal value of the height specific resistance is the height specific permeability (K).

If the material is incompressible, resistance and solids volume fraction are constant. In the case of compressible material behavior those parameters increase with higher pressure. Compressible material behavior can occur due to particle rearrangement, destruction of card house structures in the case of elongated particles, elastic and plastic deformation or breakage. [13]

To model resistance and solids volume fraction for compressible filter cakes Tiller, Kwon [15] proposed the equations

$$\alpha = \alpha_0 \left(1 + \frac{p}{p_0}\right)^N, \tag{8}$$

$$p = p_0 \left(\left(\frac{\phi}{\phi_0}\right)^\gamma - 1\right), \tag{9}$$

$$\phi = \phi_0 \left(1 + \frac{p}{p_0}\right)^\beta. \tag{10}$$

Eqs. 9 and 10 can be transformed into each other. The exponent parameters N, γ and β are fitted to experimental data. Parameters p_0, α_0 and ϕ_0 are usually set to the first available measurement point. With the sum of exponents N and β the compressibility of the particle network is characterized, if Eq. 8 is used with the height specific resistance [13]. Values close to zero mean the system is incompressible. Below one the system is identified as compressible, between one and two as highly compressible and above two as super compressible [13].

Since new engineered protein crystals are only available at low volumes (about 1 mL), standard filtration experiments using a pressure nutsche filter are not possible. Although hen egg lysozyme is easily available, ADH from *Lactobacillus brevis* is not. Therefore, experiments are carried out using an in house 3D printed filtration cell which is depicted in Fig. 4. The cuvette consists of two parts. The bottom part catches the filtrate (Fig. 4 left), the upper part holds the suspension and the filter cake (Fig. 4 right). Between those two parts sits the support structure and the filter medium. The filter area is $A_m = 51.65\,\mathrm{mm}^2$. The assembled cuvette is placed in the LUMiSizer® centrifuge and with light transmission filtration progress on the cake side is measured in situ. For easier and quicker analysis, the permeation of filter cakes was measured instead of the whole filtration process. The derived equation by Loginov et al. [30]

$$\ln\left(\frac{r_c + r_m - h_l}{r_m - r_c + h_l}\frac{r_m - r_c + h_{l,0}}{r_m + r_c - h_{l,0}}\right) = \frac{\rho_l \omega^2 r_m}{\eta\,(R_m + (r_m - r_c)\,\alpha_h)}t, \tag{11}$$

connects the distance from the centrifuge center of the membrane r_m, the filter cake top r_c and the liquid height above the filter cake h_l with material and process properties. From this equation the integral height specific resistance of the filter cake is obtained. For the detailed working principle of the cuvette and data analysis please refer to Radel et al. [19] and Loginov et al. [30]. In centrifugal filtration the pressure on the filter medium does not remain constant, but decreases with descending fluid height. Hence, all filtration related pressures mentioned are mean pressures during the filtration process.

For permeation experiments in this study, Pall (Germany) Supor® membranes with a nominal pore size of 0.2 µm and a resistance of 2.1×10^{10}–$3.6 \times 10^{10}\,\mathrm{m}^{-1}$ are used [19].

To build the filter cake approximately 500 µL of crystal suspension are filled into the cuvette and centrifugated. For the permeation experiments 300–400 µL of supernatant are gently added on the top of the prebuilt filter cake with an Eppendorf (Germany) pipette. The liquid is permeated through the filter cake at a certain rotational speed and the progress is tracked. This is repeated for different speeds up to 4000 rpm which is the maximum possible speed.

2.4. Flux Density Function

For obtaining the flux density function (f_{bk}) of protein crystals, centrifugal settling and filtration as described in the previous section is used.

In the case of solids volume fractions below the gel point ($\phi_0 < \phi_g$), a common method to measure the flux density function is to observe the settling velocity v_s at the very beginning of the settling process when the solids volume fraction is almost equal to the initial solids volume fraction ϕ_0. The gel point marks the transition from a suspension to a particulate network.

Using the relation of the flux density function for a closed system Kynch [21]

$$f_{\mathrm{bk}} = -\phi_0 v_s \text{ for } \phi_0 < \phi_g \text{ and } t \to 0, \tag{12}$$

allows calculating f_{bk} directly from the settling velocity v_s and the known initial solids volume fraction ϕ_0. The standard experimental setup to obtain the settling velocity is explained in Sec. 2.2 and can be seen in Fig. 3, which also qualitatively shows the effect of the solids volume fraction on the settling velocity.

Measuring and tracking the settling front with an optical centrifuge allows to speed the measurement up and to substantially reduce the amount of required sample volume. This however means we have to alter Eq. 12 to

$$f_{\mathrm{bk}} = -\phi_0 \frac{v_s}{Z} \text{ for } \phi_0 < \phi_g \text{ and } t \to 0. \tag{13}$$

Preprints (www.preprints.org) | NOT PEER-REVIEWED | Posted: 20 May 2021 doi:10.20944/preprints202105.0483.v1

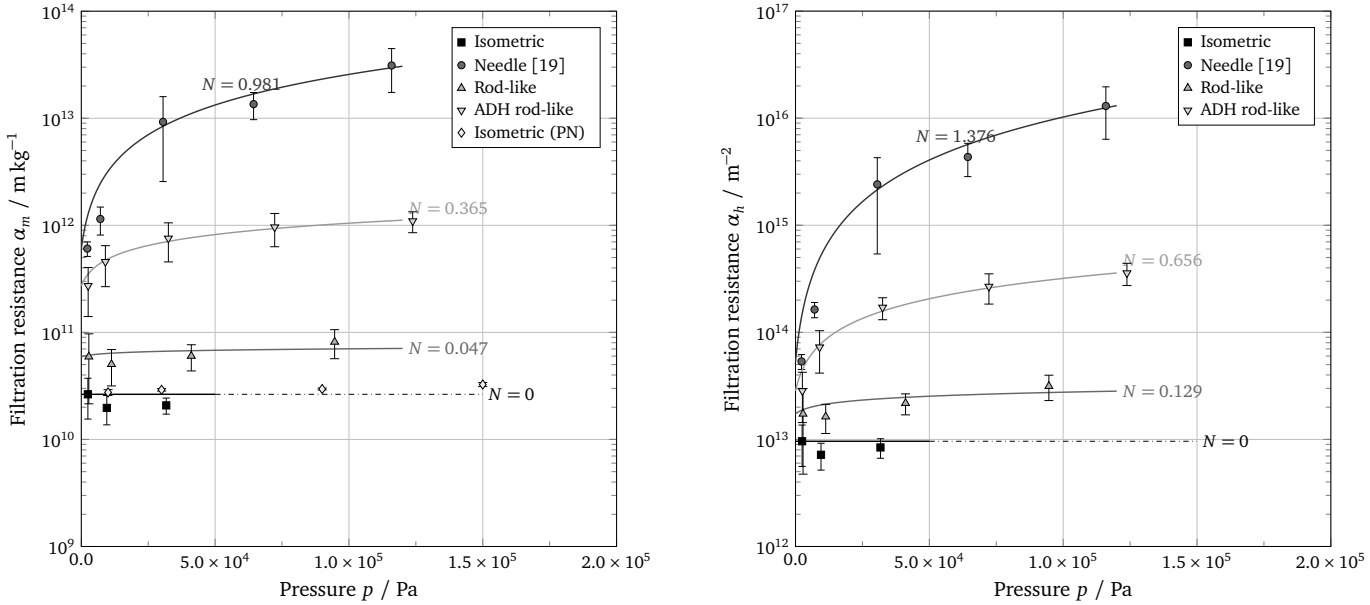

Figure 5: Left: mass specific filtration resistance for three lysozyme crystal shapes and rod-like alcohol dehydrogenase crystals; right: height specific filtration resistances for three lysozyme crystal shapes and rod-like alcohol dehydrogenase crystals; The data for needle shaped crystals was published in Radel et al. [19]; solid lines are model calculations according to Tiller, Kwon [15]

Using the resistance of a sediment or filter cake, values for flux density function above the gel point are calculated with

$$f_{\mathrm{bk}} = -\frac{\Delta\rho\, g\, \phi^2}{\alpha_h \eta} \tag{14}$$

were α_h is a function of ϕ. Determining the mean solids volume fraction and mean height specific filtration resistance with the filtration cell described in Radel et al. [19] is directly possible from the same measurement.

Ideally, joined flux density data obtained from settling and permeation experiments have only a small gap at the gel point. Obviously, the flux density function is significantly higher when considering permeation than during settling.

3. Results

3.1. Permeation of filter cakes

3.1.1. Filter cake resistance

The mass specific filtration resistance obtained from permeation experiments in the centrifuge are shown in Fig. 5 left and corresponding height specific resistances are shown on the right-hand side of Fig. 5. To compare the different protein crystals with each other, the mass specific resistance is more suitable than the height specific resistance because the resistance is normalized with the particle mass. As can be seen from Fig. 5 left, the resistances of isometric and rod-like lysozyme crystals are the lowest with about 2.5×10^{10} and 5×10^{10} m kg^{-1}. Those two systems also show a low dependency of the resistance on pressure which indicates low compressibility. The highest possible pressure for the isometric crystals is below 0.5×10^5 Pa resulting in only three data points. At higher revolutions the start-up of the centrifuge takes too long so that all the liquid is already permeated before the desired revolutions per minute have been reached. Therefore, results obtained with a VDI 2762 [18] nutsche filter (diamonds, Isometric PN) are shown for comparison. As can be seen, the results from the pressure nutsche are in very good agreement with the three data points from centrifugal filtration. Although the resistance of rod-like lysozyme crystals is slightly larger than the resistance of isometric crystals, over all both systems offer low resistance and are hence easy to filtrate. For rod-like ADH crystals on the other hand the resistance is about one magnitude larger ranging from 2.7×10^{10}–1.1×10^{11} m kg^{-1} and shows a slight dependency on the pressure. This indicates compressible material behavior and less efficient filtration.

Needle shaped lysozyme crystals show the highest resistances in the range of 6.1×10^{11}–3.1×10^{13} m kg^{-1} spreading over two magnitudes. Obviously, this means the filtration process is quite slow compared to the other crystalline systems. Since the resistance increases strongly at higher pressures, the process does not become much faster or efficient when using higher filtration pressures. An increase in resistance this large may be explained by destruction of card house structures in the filter cake and is also a strong indicator for particle breakage [12].

The solid lines show the calculated curves according to Tiller, Kwon [15] from Eq. 8. For the isometric lysozyme crystals the extrapolated values are shown in the dash dotted curve. As can be seen, the curves give a good representation of the measurement data. The corresponding values for the exponent N ranges from 0 for the isometric crystals to 0.981 for the lysozyme needles. This also shows the strong

Preprints (www.preprints.org) | NOT PEER-REVIEWED | Posted: 20 May 2021 doi:10.20944/preprints202105.0483.v1

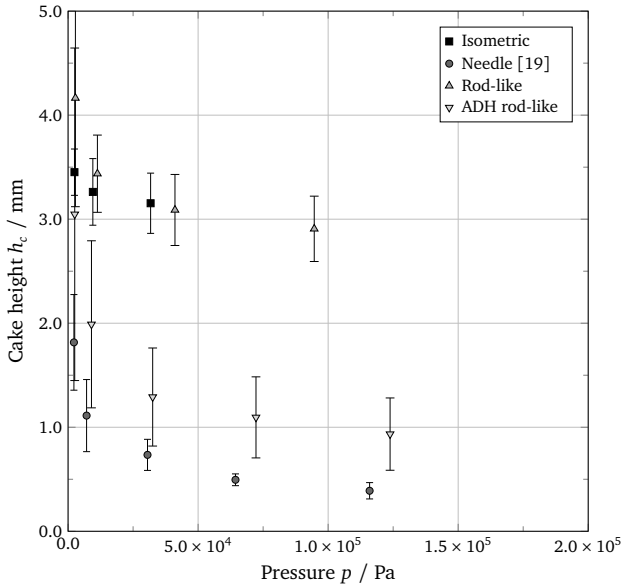

Figure 6: Filter cake height of the three lysozyme crystal shapes and rod-like ADH crystals

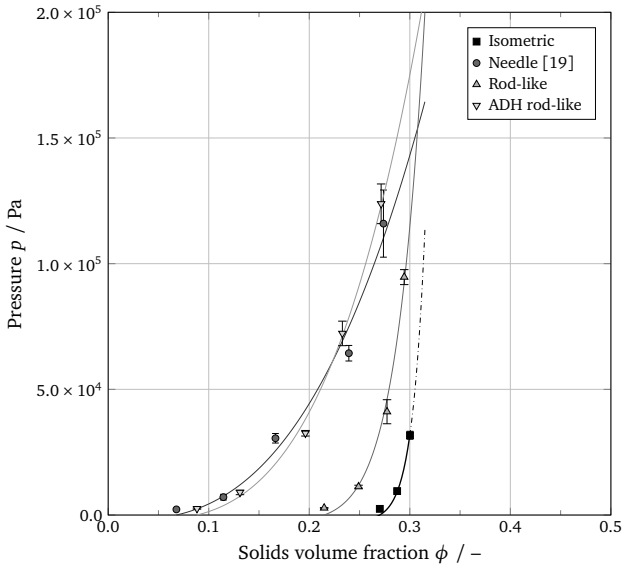

Figure 7: Filtration pressure of the crystalline systems dependent on the solids volume fraction

differences in filter cake compressibility between the different particle systems.

However, to characterize compressibility and for calculating flux density function, the height specific resistance on the right-hand side of Fig. 5 is more suitable because it can be directly inserted into Eq. 14. As can be seen, the gap between ADH and the lysozyme crystals is much smaller at low pressures but the tendency is the same. The model fits are calculated analogous to the left-hand side of the Figure with values of N ranging from 0 for the isometric crystals over 0.129 for rod-like to 0.656 for ADH to over 1.376 for needle shaped crystals. Those fits also provide a good representation of the measured data points.

3.1.2. Filter cake height

The filter cake height of the crystalline systems is directly available from the measurements with the filtration cell because the cake position is always visible and provides a characteristic peak in the transmission profiles. In Fig. 6 the filter cake heights over filtration pressure for the investigated crystal systems are shown. As can be seen from Fig. 6, the tendency towards slightly smaller cake heights with increasing pressure is observed for rod-like lysozyme crystals. The same is true for rod-like ADH crystals but the tendency is much more distinct. The most significant decrease in filter cake height is again observed for the needle shaped lysozyme crystals. For those crystals the height decreases from 1.8 mm at 0.22×10^5 Pa to 0.39 mm at 1.16×10^5 Pa.

The big error bars for ADH crystals are due to the small available amount of sample and its low initial solids volume fraction. That is why small portions of original ADH suspension have been centrifugated at low centrifugal forces to concentrate the particles without introducing breakage or crystal aggregation. After carefully removing supernatant from the centrifugated sample, the solids volume fraction of the now concentrated suspensions scatter. That is why the initial cake heights and the initial solids volume fractions for ADH are scattered over a larger range compared to the lysozyme crystals.

The data points also scatter more at lower pressures because the particles tend to smear the glass window of the filtration cell which leads to more uncertainty of the filter cake position.

3.1.3. Filtration pressure

The knowledge of cake height allows to calculate the corresponding integral solids volume fraction in the filter cake. The filtration pressure vs. solids volume fraction is depicted in Fig. 7. For the more compressible systems (needle lysozyme and ADH) the curves show a slow increase of pressure with higher solids volume fractions. In the case of the more incompressible particle systems (isometric and rod-like lysozyme) the increase in pressure is much steeper. For an ideal incompressible particle system the pressure would jump from zero to infinity at the gel point.

The calculated fits according to Eq. 9 show good agreement with measurement results. For the isometric crystals the extrapolated values of the dash dotted curve might not be completely accurate. In general, extrapolating is critical due to the exponential nature of the pressure on solids volume fraction dependency. Also, particle systems typically have a maximum solids volume fraction $\phi_{\max}$ at which further compression is impossible. This is currently not reflected in the applied model.

Table 2 shows the calculated parameters for the fit exponents and the sum of $N(\alpha_h) + \beta$. This sum is useful to classify the compressibility of the four particle systems according to Alles, Anlauf [13]. The isometric crystals are considered incompressible with an exponent sum of 0.04. Rod-like

Preprints (www.preprints.org) | NOT PEER-REVIEWED | Posted: 20 May 2021 doi:10.20944/preprints202105.0483.v1

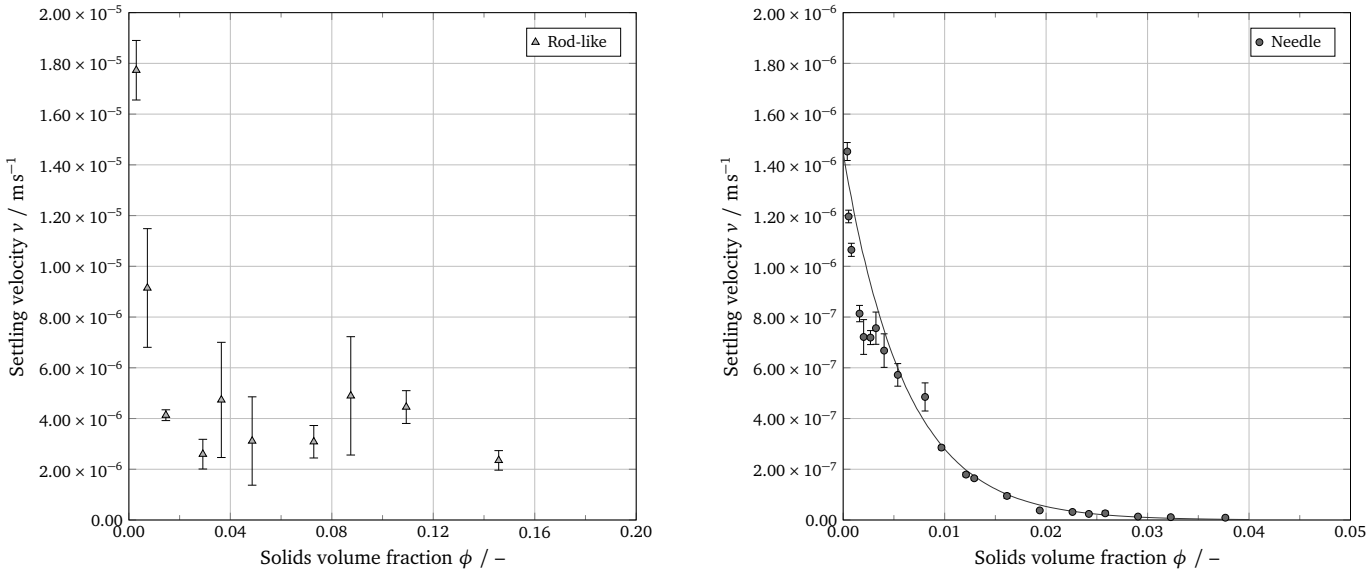

Figure 8: Settling velocities for rod-like lysozyme crystals (left, triangles) and needle shaped lysozyme crystals (right, circles); Velocities for needle shaped lysozyme are calculated values of the settling velocity in earth gravity.

lysozyme and ADH crystals are compressible particle systems, with ADH being significantly more compressible than rod-like lysozyme. Needle shaped lysozyme with a sum of 1.73 is highly compressible and close to super compressibility [19].

From those results it becomes evident that the particle shape of the four crystal systems has a high influence on filterability. The best filtration properties exhibit isometric and rod-like lysozyme crystals because they have low filtration resistance and thus enable fast filtration. Also, those particle systems have high solids volume fractions which means less residual moisture in the filter cake and hence better dewatering properties. ADH and needle shaped lysozyme crystals on the other hand show compressible material behavior and have high resistances compared to the other two particle systems. The solids volume fraction at lower pressures is much smaller which means that more fluid remains in the pores of the filter cake. Thermal drying of filter cakes with crystalline systems is difficult because the dissolved protein in the pore fluid crystallizes when the fluid evaporates and thus blocks the pores needed to transport the evaporated gas.

3.2. Settling

For two of the discussed crystal systems settling velocities in earth gravity (rod-like lysozyme) and in the centrifugal field (needle shaped lysozyme) have been determined. The isometric crystal suspension did not show a clear settling front so that the results are inconclusive. The available sample volume for ADH did not allow a thorough analysis of settling behavior.

Table 2: Exponents of the fits according to Tiller, Kwon [15] from Eqs. 8, 9 and 10

Crystal system	$N(\alpha_h)$	β	γ	$N+\beta$
Isometric	0	0.038	25.003	0.04
Needle	1.376	0.356	2.806	1.73
Rod-like	0.129	0.089	11.173	0.22
ADH	0.656	0.288	3.469	0.94

Fig. 8 shows on the left-hand side the settling velocities for different solids volume fractions for rod-like lysozyme crystals. On the right-hand side settling velocities for the needle shaped lysozyme crystals are shown.

To make the results from centrifugal settling experiments comparable with the other particle system, the velocities have been recalculated according to

$$v_g = \frac{v_C}{Z}. \tag{15}$$

with v_C being the settling velocity in the centrifugal field and v_g being the settling velocity in earth gravity. The definition of Z is given in Eq. 4.

For both particle systems the settling velocity decreases in the order of approximately one magnitude with increasing solids volume fraction. In the case of rod-like crystals the maximum settling velocity is $17.7 \times 10^{-6}\,\mathrm{m\,s^{-1}}$ at the lowest solids volume fraction of 0.003. The velocity then quickly drops to around $4.0 \times 10^{-6}\,\mathrm{m\,s^{-1}}$ at solids volume fractions above 0.014 and remains almost constant for solids volume fractions up to 0.146.

In the case of the lysozyme needles, the initial settling velocity is about $1.45 \times 10^{-6}\,\mathrm{m\,s^{-1}}$ at a solids volume fraction of 0.0004. Settling velocity then decreases slowly to a final value of about $0.003 \times 10^{-6}\,\mathrm{m\,s^{-1}}$ at ϕ=0.019 and remains almost constant till the maximum solids volume fraction of 0.038.

The decrease of settling velocities in both particle systems is due to hindered settling in a particle collective. At low solids volume fractions single particle settling as described by

Preprints (www.preprints.org) | NOT PEER-REVIEWED | Posted: 20 May 2021 doi:10.20944/preprints202105.0483.v1

Stokes is thus much faster than hindered settling at higher solids volume fractions.

The maximum solids volume fraction, which could be achieved with concentration of the particle systems, is for the rod-like crystals with 0.146 almost four times bigger than for the needle shaped crystals with 0.038. This also reflects in the big gap of solids volume fraction for those both crystal shapes in Fig. 7. The gel point for lysozyme needles must hence be much lower than for rod-like lysozyme crystals.

Also, the total drop in settling velocity is for needle shaped lysozyme crystals with a factor of 161 much larger than for the rod-like crystals where the settling velocity drops at a factor of about 7.5. The influence of solids volume fraction on settling velocity is thus for the lysozyme needles much more dominant than for the rod-like crystals. It is also interesting to see that with settling experiments the solids volume fraction of lysozyme needles reaches 0.038 but in filtration this particle system is compressed to a solids volume fraction of 0.274 (see Fig. 7). This corresponds to a 7.2 fold increase in solids volume fraction. This can be explained by the destruction of card house structures in the filter cake to a more compact cake and also by crystal breakage. Cornehl et al. [10] have analyzed lysozyme crystal breakage. They found that even at low pressures in typical filtration processes, crystal breakage occurs which worsens filtration and dewatering properties.

The solid line in Fig. 8 right shows a modified fit based on Richardson, Zaki [28] (see Eq. 3). Since the model of Richardson and Zaki assumes spherical particles, adjustments for needle shaped particles are necessary. Instead of using the default exponent 4.65, the exponent m is calculated with respect to measured experimental data and gives 163.4. Such a curve can not be calculated for the rod-like particles because of the atypical, almost constant, settling velocities in the range of solids volume fractions from 0.04 to 0.147.

3.2.1. Flux density function

With the results from the previous sections, especially with the calculated fit models from Richardson, Zaki [28] and Tiller, Kwon [15], the flux density function can be calculated as follows

$$f_{\mathrm{bk}} = \begin{cases} -\phi v_s (1-\phi)^m & \text{for } \phi < \phi_g \\ -\frac{\Delta\rho g \phi^2}{\alpha_{h0}\left(\left(\frac{\phi}{\phi_0}\right)^{\gamma}\right)^N \eta} & \text{for } \phi_g \leq \phi \end{cases} . \tag{16}$$

Fig. 9 shows the complete flux density function for the needle shaped particle system. The gel point is not exactly known but expected to lie somewhere between 0.03 and 0.06. The dashed line in Fig. 9 is the calculated flux density function according to the modified Richardson and Zaki model (first segment of Eq. 16). The dash dotted line is calculated based on permeation data with the models of Tiller. The last five data points in Fig. 9 are obtained with permeation experiments, the other data points at lower solids volume fractions are determined with settling experiments.

Fig. 10 shows the flux density function for solids volume fractions above the gel point for needle shaped lysozyme and

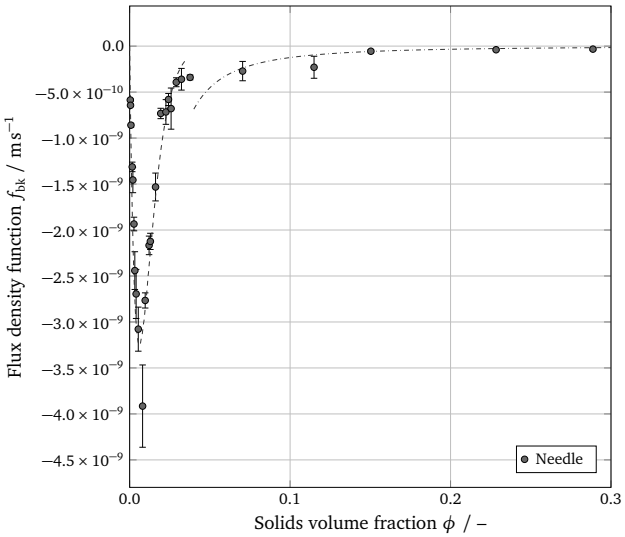

Figure 9: Flux density function for needle shaped lysozyme particles

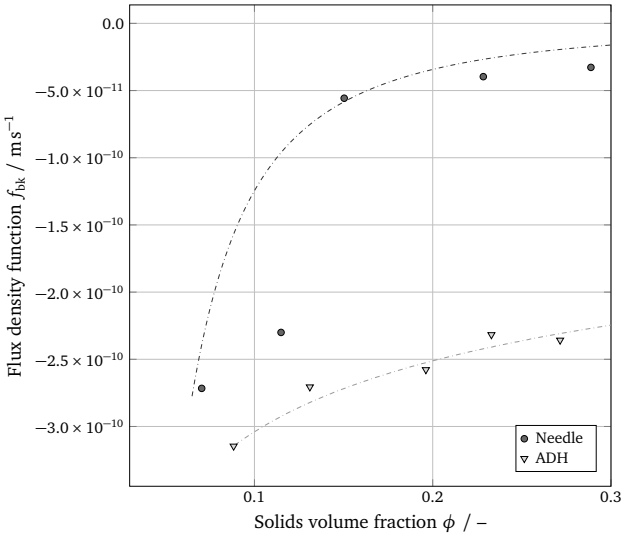

Figure 10: Flux density function for needle shaped lysozyme and ADH at solids volume fractions above the gel point

ADH crystals calculated from permeation data. As can be seen the flux density of ADH crystals is much smaller than the flux density of needle shaped lysozyme which is due to the lower filter cake resistance of ADH. The model describes the measured data well except for the second data point of the needle shaped lysozyme.

The flux density function allows to model the settling and permeation behavior of a particle system only in dependency of the solids volume fraction. This is especially useful for processes in which both effects play a significant role. Also in simulation models, for instance in Bürger, Concha [31], the flux density function is used as an input parameter for the simulation of settling processes.

 doi:10.20944/preprints202105.0483.v1

4. Conclusion

The settling and permeation behavior for different protein crystal systems can be analyzed on a small scale using a 3D printed filtration cell and an analytical optical centrifuge. The crystal shape has a big influence on the filtration and settling properties. Being able to characterize filtration and settling on a small scale allows testing different crystal shapes or crystal modifications early in process development. Using the flux density function, the whole settling and permeation process can be modeled in dependency of the solids volume fraction. For solids volume fractions below the gel point this requires the ability to observe a distinct settling front. This is not possible for all particle systems, but for example in the case of the needle shaped lysozyme crystals. Above the gel point the flux density function can be obtained with permeation experiments on a small scale with only about 300 µL of supernatant per experiment.

The flux density function may then be used in computer simulations where settling and also permeation of a particulate network occur. This is for instance the case in a chamber filter press.

Conflict of Interest

The authors declare that there is no conflict of interest to disclose.

Acknowledgment

The authors thank the German Research Foundation (DFG) for funding the project NI 414/26-1, NI 414/26-2 and the DiSPBiotech priority program (SPP 1934). Prof. Kind and Dr.-Ing. Michael Barros-Groß from the institute of thermal process engineering at the KIT are thanked for providing crystalline proteins. Prof. Weuster-Botz and Dr. Phillip Grob of the institute for biochemical engineering at Technical University of Munich are thanked for providing the protein alcohol dehydrogenase from *Lactobacillus brevis*.

Preprints (www.preprints.org) | NOT PEER-REVIEWED | Posted: 20 May 2021 doi:10.20944/preprints202105.0483.v1

Nomenclature

Symbol	Description
Latin Symbols	
A	area (mm^2)
f_{bk}	flux density function ($m\,s^{-1}$)
g	gravity ($m\,s^{-2}$)
h	height (mm)
K	specific permeability (m^2)
p	pressure (Pa)
Q	cumulative particle size distribution (–)
R	resistance (m^{-1})
r	distance from centrifuge center (mm)
t	time (s)
V	volume (m^3)
v	velocity ($m\,s^{-1}$)
x	particle diameter (µm)
Z	relative centrifugal acceleration (–)
Greek Symbols	
α_m	mass specific resistance ($m\,kg^{-1}$)
α_h	height specific resistance (m^{-2})
ϵ	porosity (–)
η	dynamic viscosity (Pa s)
ω	angular frequency (s^{-1})
ϕ	solids volume fraction (–)
ϕ_0	solids volume fraction at $p = p_0$ (–)
ρ	density ($kg\,m^{-3}$)
Subscripts	
0	inital value (–)
c	filter cake related (–)
g	gel point related (–)
l	liquid related (–)
m	filter medium related (–)
s	suspension/solids related (–)

 doi:10.20944/preprints202105.0483.v1

References

[1] Jen A, Merkle HP. Diamonds in the rough: Protein crystals from a formulation perspective. Pharm. Res. 2001; 18:1483–1488.

[2] Basu SK, Govardhan CP, Jung CW, Margolin AL. Protein crystals for the delivery of biopharmaceuticals. Expert Opin. Biol. Ther. 2004; 4:301–317.

[3] Hubbuch J, Kind M, Nirschl H. Preparative Protein Crystallization. Chemical Engineering & Technology. 2019; 42:2275–2281.

[4] Hekmat D. Large-scale crystallization of proteins for purification and formulation. Bioprocess. Biosyst. Eng. 2015; 38:1209–1231.

[5] Nowotny P, Hermann J, Li J, Krautenbacher A, Klöpfer K, Hekmat D, Weuster-Botz D. Rational Crystal Contact Engineering of Lactobacillus brevis Alcohol Dehydrogenase to Promote Technical Protein Crystallization. Cryst. Growth Des. 2019.

[6] Hermann J, Nowotny P, Schrader TE, Biggel P, Hekmat D, Weuster-Botz D. Neutron and X-ray crystal structures of Lactobacillus brevis alcohol dehydrogenase reveal new insights into hydrogen-bonding pathways. Acta Crystallographica Section F: Structural Biology Communications. 2018; 74:754–764.

[7] Kubiak M, Solarczek J, Kampen I, Schallmey A, Kwade A, Schilde C. Micromechanics of Anisotropic Cross-Linked Enzyme Crystals. Cryst. Growth Des. 2018; 18:5885–5895.

[8] Grob P, Huber M, Walla B, Hermann J, Janowski R, Niessing D, Hekmat D, Weuster-Botz D. Crystal Contact Engineering Enables Efficient Capture and Purification of an Oxidoreductase by Technical Crystallization. Biotechnol. J. 2020; 15:2000010.

[9] Kubiak M, Storm KF, Kampen I, Schilde C. Relationship between Cross-Linking Reaction Time and Anisotropic Mechanical Behavior of Enzyme Crystals. Cryst. Growth Des. 2019; 19:4453–4464.

[10] Cornehl B, Overbeck A, Schwab A, Büser JP, Kwade A, Nirschl H. Breakage of lysozyme crystals due to compressive stresses during cake filtration. Chem. Eng. Sci. 2014; 111:324–334.

[11] Cornehl B, Grünke T, Nirschl H. Mechanical Stress on Lysozyme Crystals during Dynamic Cross-Flow Filtration. Chem. Eng. Technol. 2013:1665–1674.

[12] Anlauf H. Wet Cake Filtration: Fundamentals, equipment, strategies. Weinheim: WILEY VCH, 2020.

[13] Alles CM, Anlauf H. Filtration mit kompressiblen Kuchen: Effiziente Konzepte für eine anspruchsvolle Trennaufgabe. Chem. Ing. Tech. 2003; 75:1221–1230.

[14] Tiller FM, Hsyung NB. Unifying the theory of thickening, filtration, and centrifugation. Water Sci. Technol. 1993; 28:1–9.

[15] Tiller FM, Kwon JH. Role of porosity in filtration: XIII. Behavior of highly compactible cakes. AIChE J. 1998; 44:2159–2167.

[16] Tarleton ES. Predicting the performance of pressure filters. Filtr. Sep. 1998; 35:293–286.

[17] Capellades G, Neurohr C, Azad M, Brancazio D, Rapp K, Hammersmith G, Myerson AS. A Compact Device for the Integrated Filtration, Drying, and Mechanical Processing of Active Pharmaceutical Ingredients. J. Pharm. Sci. 2020; 109:1365–1372.

[18] VDI 2762. Mechanical solid-liquid separation by cake filtration. Standard VDI 2762. Verein Deutscher Ingenieure, 2010.

[19] Radel B, Funck M, Nguyen TH, Nirschl H. Determination of filtration and consolidation properties of protein crystal suspensions using analytical photocentrifuges with low volume samples. Chem. Eng. Sci. 2019; 196:72–81.

[20] Loginov M, Samper F, Gésan-Guiziou G, Sobisch T, Lerche D, Vorobiev E. Centrifugal ultrafiltration for determination of filter cake properties of colloids. J. Membr. Sci. 2017; 536:59–75.

[21] Kynch GJ. A theory of sedimentation. Trans. Faraday Soc. 1952; 48:166.

[22] Bürger R, Concha F, Tiller FM. Applications of the phenomenological theory to several published experimental cases of sedimentation processes. Chemical Engineering Journal. 2000; 80:105–117.

[23] Barros Groß M, Kind M. Comparative Study on Seeded and Unseeded Bulk Evaporative Batch Crystallization of Tetragonal Lysozyme. Cryst. Growth Des. 2017; 17:3491–3501.

[24] Barros Groß M, Kind M. From microscale phase screening to bulk evaporative crystallization of proteins. J. Cryst. Growth. 2018; 498:160–169.

[25] Kundrot CE, Richards FM. Effect of hydrostatic pressure on the solvent in crystals of hen egg-white lysozyme. J. Mol. Biol. 1988; 200:401–410.

[26] EN ISO 15212-1. Oscillation-type density meters - Part 1: Laboratory instruments. Standard EN ISO 15212-1. European Committee for Standardization, 1999.

[27] ISO 12154. Determination of density by volumetric displacement - Skeleton density by gas pycnometry. Standard ISO 12154. International Organization for Standardization, 2014.

[28] Richardson JF, Zaki WN. Sedimentation and fluidisation: Part I. Chem. Eng. Res. Des. 1997; 75.

[29] Lerche D, Sobisch T. Consolidation of concentrated dispersions of nano- and microparticles determined by analytical centrifugation. Powder Technol. 2007; 174:46–49.

[30] Loginov M, Lebovka N, Vorobiev E. Multistage centrifugation method for determination of filtration and consolidation properties of mineral and biological suspensions using the analytical photocentrifuge. Chem. Eng. Sci. 2014; 107:277–289.

[31] Bürger R, Concha F. Mathematical model and numerical simulation of the settling of flocculated suspensions. Int. J. Multiphase Flow. 1998; 24:1005–1023.